# Sea surface salinity reemergence in an updated North Atlantic in-situ salinity data set

Claude Frankignoul, Élodie Kestenare, Gilles Reverdin

# Sea surface salinity reemergence in an updated North Atlantic in-situ salinity data set

Claude Frankignoul,[a] Elodie Kestenare,[b] Gilles Reverdin [a]

[a] *Sorbonne Université, IRD/MNHN/CNRS, LOCEAN, Paris, France*
[b] *University of Toulouse III, IRD/CNRS/CNES, LEGOS, Toulouse, France*

*Corresponding author address* : Claude Frankignoul, claude.frankignoul@locean.ipsl.fr

## Abstract

Monthly sea surface salinity (SSS) fields are constructed from observations, using objective mapping on a 1°x1° grid in the Atlantic between 30°S and 50°N in the 1970-2016 period in an update of the data set of Reverdin et al. (2007). Data coverage is heterogeneous, with increased density in 2002 when Argo floats become available, high density along Voluntary Observing Ship lines, and low density south of 10°S. Using lag correlation, the seasonal reemergence of SSS anomalies is investigated between 20°N and 50°N in 5°x5° boxes during the 1993-2016 period, both locally and remotely following the displacements of the deep mixed-layer waters estimated from virtual float trajectories derived from the daily AVISO surface geostrophic currents. Although SSS data are noisy, local SSS reemergence is detected in about half of the boxes, notably in the northeast and southeast, while little reemergence is seen in the central and part of the eastern subtropical gyre. In the same period, sea surface temperature (SST) reemergence is found only slightly more frequently, reflecting the short data duration. However, taking geostrophic advection into account degrades the detection of remote SSS and even SST reemergence. When anomalies are averaged over broader areas, robust evidence of a second and third SSS reemergence peak is found in the northeastern and southeastern parts of the domain, indicating long cold-season persistence of large-scale SSS anomalies, while only a first SST reemergence is seen. An oceanic reanalysis is used to confirm that the correlation analysis indeed reflects the reemergence of subsurface salinity anomalies.

## 1. Introduction

Namias and Born (1970) first noted a tendency for North Pacific sea surface temperature (SST) anomalies to recur from one winter to the next while disappearing during summer, which substantially increased their persistence. They speculated that the deep winter mixed layer temperature anomalies remained under the shallow seasonal thermocline during summer and were insulated from surface heat exchanges with the atmosphere before being re-entrained into the surface layer during mixed-layer deepening in fall and early winter. This mechanism was further investigated, among others, often by including reanalyzed subsurface temperature data to follow the SST evolution under the seasonal thermocline, in the North Pacific by Alexander and Deser (1995) and Alexander et al. (1999, 2001) and in the North Atlantic by Watanabe and Kimoto (2000) and Timlin et al. (2002). These studies showed that reemergence was stronger when the difference between the depth of the mixed layer in winter and summer was larger. Furthermore, Deser et al (2003) extended the stochastic climate model of Frankignoul and Hasselmann (1977) to the case of a seasonally varying upper-ocean mixed depth. Hanawa and Sugimoto (2004) documented SST reemergence in the world ocean, and found that reemergence was seen when the seasonal variations in mixed-layer depth exceeded 100 m (see also Deser et al. 2003). De Coëtlogon and Frankignoul (2003) showed that advection by the mean ocean circulation could lead to nonlocal reemergence in the western subtropical and subpolar North Atlantic, and Sugimoto and Hanawa (2007) discussed remote reemergence in the North Pacific. In these studies, reemergence was clearly detected in western subtropical and subpolar regions, but it was generally not seen in the eastern subtropical oceans and in the southwestern subtropics. Several factors have been suggested to explain the lack of reemergence in the latter regions: too small seasonal range of mixed-layer depth, large fraction of mixed-layer water permanently subducted in the ocean interior, strong oceanic heat loss, and, for the North Atlantic Madeira mode water (Sugimoto and Hanawa 2005), vigorous salt-finger mixing.

The fall and winter mixed layer deepening should lead to a corresponding reemergence of sea surface salinity (SSS) anomalies, but because of sparse observations there has been no observational studies of SSS reemergence. Alexander et al. (2001) considered a simulation with an atmospheric general circulation model coupled to an entraining bulk ocean mixed layer model and found that SSS reemergence was stronger than SST reemergence, presumably because SST anomalies are strongly damped by surface flux and thus persist less than SSS anomalies. Hence, it is of much interest to investigate the persistence and propagation of SSS anomalies in observations, despite data limitations. In the present paper, SSS reemergence is investigated in the North Atlantic mid-latitudes based on correlation analysis, using a new extended monthly observational data set that covers the period 1970-2016, albeit with numerous data gaps. Both local and remote reemergence are investigated in the 1993-2016 period, and, for comparison, SST reemergence is also investigated. An oceanic reanalysis is also used in the better-documented 2005-2018 period.

## 2. Data and method

### *2.1 The updated North Atlantic SSS data set*

The SSS fields constructed from observations by Reverdin et al. [2007, hereafter RKFD07] have been extended from 1970-2002 to 1970-2016 (http://dx.doi.org/10.6096/SSS-LEGOS-GRID-ATL). As described in RKFD07, the monthly SSS is gridded in 30°S-50°N using objective mapping [Bretherton et al., 1976] at 1°x1° spatial resolution. The product is mainly based on water samples and underwater thermosalinographs installed on research vessels and voluntary observing ships (VOS, http://www.legos.obs-mip. fr/observations/sss/), PIRATA moorings in the tropical

Atlantic (http://www.brest.ird.fr/pirata/), SMOS and CARIOCA drifters [G. Reverdin, personal communication], and Argo floats (http://www.coriolis.eu.org/Observing-the-ocean/Observing-system-networks/Argo). The raw SSS data were grouped in monthly 1°x1° square bins. Only grid points where the estimated RMS error (normalized by the signal amplitude) does not exceed 0.8 were retained, as in RKFD07, and grid points with too sparse observations were excluded. Figure 1a shows that the spatial coverage of SSS observations (before objective analysis) increases considerably after 2005 when Argo float data become widely available. The data coverage is heterogeneous, with high density along three Europe-South America and Europe-South Africa VOS lines and low density south of 10°S (Fig. 1b). The mean seasonal cycle is first estimated iteratively based on all available data and objective maps, as described in RKFD07. The objective mapping is sequential in time with a forward and backward scheme that incorporates all the data increments first gridded on a 1°x1° month grid with an assumed correlation function in time and space, as done in optimal interpolation. This function reproduces the estimated spatial and temporal correlation of the salinity anomalies as estimated in five subdomains and for two extended seasons that correspond to strong or weak salinity near-surface stratification (see RKFD07 for details). The same sequential approach is used for mapping the SSS anomalies obtained by subtracting the seasonal cycle, using as guess the mapped anomaly of the previous step (a month ahead or after) weighted by assuming a 2-month decay-time. Two analyses are performed, one forward and one backward, and their average used. The resulting fields are provided with a parameter that indicates the signal-to-noise ratio expected from the data distribution, thus how close the analysis is to the input data or how it is weighted by the guess field. Except in data sparse regions, the differences between the two analyses are usually smaller than the anomalies portrayed and consistent with the estimated errors. As discussed in RKFD07, mapped anomalies with an estimated relative error as large as 0.8

still seem to be retaining part of the signal, albeit with a reduced amplitude. However, anomalies with larger estimated errors were not retained. Although it generates gaps in the analyzed fields, it does not bias the lag correlation estimates.

There are several differences between the present data set and the other available SSS products, which are also based on quality-controlled data but only use vertical salinity profiles. By including the other sources of SSS observations listed above, our data set is based in the 1993-2002 period on more than twice the number of 1°x1° bins with SSS observations and a more homogeneous distribution. The differences decrease after 2005 because of the many ARGO floats, although our product still includes 20 to 30% more bins with SSS observations than products solely based on salinity profiles. This better sampling has allowed us to use a twice longer period to investigate SSS reemergence in the North Atlantic.

There are additional differences between SSS products. In EN4 (Good et al. 2004), salinity is estimated from the vertical salinity profiles by spreading the information vertically, using two correlation length scales, which are set to 200 and 100 m. This smoothing makes it particularly unsuitable for investigating SSS reemergence, which critically depends on the detailed vertical structure of salinity between the depth of the summer and the winter mixed layers. In addition, the persistence-based forecasts use a forward scheme in EN4, rather than an average of a forward and backward scheme, and it has a longer e-folding scale (9.5 months instead of 5-6 months at most), which could further blur reemergence peaks. Finally, the EN4 analysis will relax to climatology in the absence of observations, which would bias the seasonal autocorrelation, unlike in our data set where analyzed data with large estimated errors are dismissed. Because the historical (1945-2003) salinity analysis of Ishii et al. (2006), which uses salinity profiles in addition to SSS data, performed the objective analysis in a two-dimensional space and used rather short spatial (15 m in the vertical) scale, there should be negligible vertical smoothing. However, they use climatology instead of anomaly persistence as first guess, and a short temporal (15 day) correlation scale that likely results in numerous data gaps. Since the analysis of Ishii et al. (2006) also relaxes to climatology where data are sparse, and it does not cover the recent period with enhanced ARGO coverage, it seems far from optimal for our purposes.

Ocean reanalyses such as SODA3 (Carton et al. 2018), ORAS5 (Zuo et al. 2019) or GLORYS2v4 (https://marine.copernicus.eu/ GLOBAL_REANALYSIS_PHY_001_026) assimilate salinity profiles, but no other SSS observations. Hence, like EN4, they use much fewer observations to reconstruct the SSS field. In addition, the assimilation of the T/S profiles depends on specified error covariances or other assumptions that may not be optimal for studying SSS reemergence. For instance, ERAS5 uses the T/S profiles processed by EN4, and includes a constraint on SSS by nudging to climatology. However, the reanalyzed products also assimilate sea surface height and the atmospheric forcing, they are dynamically consistent, and they provide salinity values at depth. Hence, a reanalysis will be used to verify whether autocorrelation results indeed reflect SSS reemergence, but a systematic investigation would require that the well-sampled ARGO period be longer than at present.

For the present analysis, the 1°x1° objective fields were binned (averaged), after removing the mean seasonal cycle, in 5°x5° squares between 10°N and 50°N if at least 3 values (among 25) were available. Similar results are obtained if the cut-off is 2 or 4, although there would be more gaps in the latter case. The data density, as defined by the number of available data in each 5°x5° box divided by 25 (number of grid points) x 12 (number of months) x 24 (number of years), is given in Fig. 2 before (left) and after (right) objective analysis. Sampling is obviously not always as good as would be required to unambiguously detect SSS reemergence, even after objective analysis, in ways that are not easy to apprehend. The SSS anomaly time series are illustrated for a few 5°x5° boxes in Fig. 3, both before (yellow) and after (blue) objective analysis. The raw data are often noisy as they represent an average of much fewer values, although series based on the medians rather than the means (not shown) have smaller variance and are closer to the time series derived from the objective analysis. Data gaps are often concentrated in the 90s, as illustrated for boxes b and e in Fig. 3. Note that it was verified that spikes such as the negative one in 2001 for the 45°-50°N, 50°-45°W box (Fig. 3a) are not due to observing/instrumentation errors but reflect true fluctuations that might be undersampled and on scale smaller than the 5°x5° month boxes. In some of the boxes, the anomalies have a small trend. In addition, many boxes are dominated by low-frequency fluctuations, as in Fig. 3a, b, and f. Eddy noise can also be prevalent, as shown during the first decade by the raw SSS data in the vicinity of the Gulf Stream (Fig. 3c), when the spatial coverage was limited. Removing a quadratic polynomial by least squares fit to the monthly time series often satisfactorily removes the trend, but because the time series are short (24 years), it can also introduce unwanted behavior and mask reemergence when the low-frequency variability is large. Hence, in the following we systematically investigate reemergence with both detrended (by a linear or quadratic polynomial removed from each of the available 1°x1° time series after objective analysis, but before averaging in boxes) and non-detrended data. Several larger domains (see Fig. 7 below) were also considered to reduce data noise and focus on larger-scale anomalies, thus allowing us to search for evidence of additional reemergence peaks.

### *2.2 Other data*

Monthly sea surface temperature (SST) anomalies on a 1°x1° grid, which were obtained by an optimal interpolation of satellite and in-situ SST observations (Reynolds et al. 2002) are taken from the NOAA/OAR/ESRL PSD site (www.esrl.noaa.gov/psd). We use altimeter geostrophic currents produced by Ssalto/Duacs (AVISO, CNES) and distributed by Copernicus Marine Systems (https://resources.marine.copernicus.eu product_id=SEALEVEL_GLO_PHY_L4_REP_OBSERVATIONS_008_047). The surface geostrophic currents span the period January 1993 to December 2016 and correspond to Ssalto/Duacs gridded absolute geostrophic velocities. They have daily resolution on a 1/3°x1/3° grid. Details of the mapping technique used to derive the 1/3° gridded data are given by Dibarboure et al (2011), who show that this data set resolves wavelengths greater than 150 km with a temporal resolution of 20 days. We also used the monthly mixed layer depth climatology of Sallée et al. (2021) and salinity fields from the 1993-2018 Mercator Ocean GLORYS2V4 reanalysis at 1 degree resolution with 75 vertical levels. (https://marine.copernicus.eu/ GLOBAL_REANALYSIS_PHY_001_026).

### *2.3 Estimating advection effects*

To take into account advection effects that could lead to non-local SSS or SST reemergence by displacing the deep mixed-layer waters after they are capped by the seasonal thermocline, we use the daily estimates of the AVISO surface geostrophic currents. Geostrophic currents are used for simplicity because the wind-driven Ekman currents are primarily limited to the mixed layer above the seasonal thermocline and should not advect the water below it. However, in fall and winter when the surface layer is deep and well mixed, Ekman advection may contribute to its displacements. Also, use of surface geostrophic currents neglects their vertical shear in the upper ocean and may overestimate advection estimates, in particular during summer. In reality, interior water flows along isopycnal surfaces, so the use of surface geostrophic currents also neglects vertical advection, which may be large in regions with strong subduction or obduction. For each starting month, the position of 1381 virtual floats issued on the 1°x1° grid of a more limited domain that avoids proximity to the continental shelf and the Gulf Stream is estimated in forward mode during the following 2-year period. For instance, for a March starting date, a first run estimates a virtual float trajectory *F* from March 1, 1993 to February 28, 1995, a second run that from March 1, 1994 to February 29, 1996, and similarly until the last run that goes from March 1, 2014 to February 29, 2016. This provides 22 24-month trajectories *R* for each virtual float *F*. For each 5° x 5° box, 22 sets of averaged 24-month trajectories can be estimated by averaging over the floats issued from it, and a mean trajectory estimated by averaging them (Fig. 4).

*2.4 Detecting reemergence*

Reemergence is investigated in the 20°N–50°N domain using lag seasonal SSS anomaly autocorrelation functions starting in late winter when the mixed layer is very deep. The calculation is given for the 1993-2016 period because of better sampling and geostrophic current availability. However, extreme sparsity obscures reemergence, and indeed clear reemergence was seldom seen in boxes with limited early data density before objective analysis. For local calculations (no advection), the lag auto-correlation at each grid point and lag is based on all available data pairs (for instance between each March and each of the following Aprils), which does not require that the data be available in other months. In the SSS case, the number of pairs may thus slightly depend on lag and starting month. Non-local reemergence is estimated similarly, but along the time-varying trajectories, as described in section 3b.

The statistical signature of reemergence is a fast decrease during spring of the lag seasonal correlation with the late winter value, a correlation minimum in summer when the seasonal thermocline inhibits exchanges with the deeper waters and the shallow mixed layer strongly responds to the atmospheric forcing, a correlation increase during fall when the mixed layer depth increases and entrainment is large, and a correlation peak in early winter. Because reemerged SST anomalies are damped by the surface heat fluxes, the SST reemergence peak could occur before that of SSS, and be smaller. There should be some geographical variability in timing linked to the seasonal cycle of the mixed layer depth, which occurs earlier in the southwestern boxes (de Boyer Montégut et al. 2007; Carton et al. 2008). As illustrated in Fig. A1, the maximum mixed layer depth is largest in the northern part of the domain and over the northern flank of the subtropical gyre, and it is smallest in the northwestern and southwestern boxes. The maximum depth occurs around February and the minimum depth around July, except in some southern boxes where the maximum depth is reached in December and the minimum in May. The range of mixed layer variations (maximum minus minimum, Fig. A2) thus varies between more than 100 m in the northeastern part of the domain, more than 200 m south of the North Atlantic current, and barely more than 20 m in the four southwestern-most boxes. South of 20°N, the seasonal range is typically of the order of 20m, with some scatter in the month of minimum depth due to the seasonal changes in winds and clouds over the tropics (Carton et al. 2008).

As each starting date may be differently affected by data noise, we have considered February, March and April as starting month for estimating the seasonal autocorrelations at each location. Both original and quadratically detrended data are considered when assessing the presence of reemergence, without requiring that it be seen on both cases. In total, reemergence is thus assessed from 6 different (3 starting months, with and without detrending), albeit correlated, seasonal autocorrelations functions. Yet, its occurrence (or not) cannot always be robustly established, as discussed below. A caveat of the correlation analysis is that a peak attributed to reemergence may in some cases be due to coincident atmospheric forcing. Murata et al. (2020) showed that an early fall heating or anomalous northward advection occurring by chance where the SST was anomalously warm in the preceding winter could lead to a recurrence that was not due to entrainment. Although it is hoped that such occurrences would not substantially affect results based on 24 years of data, they may explain occasional departures from the expected statistical signature of reemergence and, perhaps, lead to a few misinterpretations. Nonetheless, the SSS reemergence suggested by the correlation analysis was verified at two locations using subsurface salinity values provided by the

GLORYS2V4 reanalysis in the better-sampled 2005-2018 period. It is also noted that reemergence only occurs if sufficiently large anomalies are present during the previous winter, so that reemergence is not a regular occurrence, as discussed in Taws et al. (2010).

## 3. SSS and SST anomaly reemergence in the 70°-20°W, 20°-50°N domain

### *a. No advection*

The seasonal autocorrelations of the SSS anomalies were examined for each box between 70°W and 20°W for a February, March, and April starting month, with and without detrending. To illustrate how they were used to assess SSS reemergence, the seasonal SSS autocorrelations for a March starting date and lag increasing from 0 (month 3 in the abscissa) to 20 (month 24) are shown in Fig. 5 (red curves) for several boxes in three latitudinal bands, where we use data with or without detrending primarily on the basis of their behavior at long lags. The corresponding seasonal SST autocorrelations (blue curves) are briefly discussed below. The boxes were in part arbitrarily chosen to illustrate a variety of situations, but all the boxes between in the 40°-45°N (30°-35°N) latitudinal bands are considered in Fig. 6 (Fig. A3), providing a more systematic view of local SSS reemergence. Because the sample is limited and the SSS anomalies are noisy, the statistical signature of reemergence is often ambiguous, leading to unavoidable subjectivity in our assessment. Moreover, the lagged autocorrelation peak is only marginally significant in some cases (the one-sided 10% (5%) significance level is 0.27 (0.34) for complete data), in part because of low-frequency contamination and data noise. Note that reemergence in Fig. 5 and A3, which are based on a March starting date, may be clearer with a February or April starting month, while the starting month in Fig. 6 is chosen to best illustrate SSS reemergence.

A clear example of SSS reemergence is found in the northeastern box (45°-50°N, 25°-20°W), which is relatively well sampled (Fig. 2) and where the climatological winter mixed layer exceeds 200 m (Fig. A1) and the seasonal range of mixed layer depth is ~ 170 m (Fig. A2), thus providing favorable conditions for reemergence. As shown for a March starting month in Fig. 5e, the seasonal autocorrelation rapidly decreases with increasing lag from March to August, shortly after the mixed layer reaches its minimum depth. The autocorrelation then increases to reach a broad peak between November to January, and it decreases again, quite rapidly after March. This evolution is consistent with a maximum entrainment rate in November/December (Carton et al. 2018). At larger lag, there is a second autocorrelation minimum in the following August followed by another increase in late fall, suggesting a second reemergence. Similar results are found for a February or April starting month, indicating robustness. Note that these seasonal variations are superposed on a slow decay that reflects low-frequency variations and the long SSS memory at this location. In our summary assessment (Fig. 7a), this box is shown in purple, which indicates clear reemergence.

Although the mixed layer conditions are similar in the adjacent box to the west (30°-25°W, 45°-50°N, Fig. 5d) and data sampling is only slightly poorer (Fig. 2), there is no indication of SSS reemergence for neither March nor April starting month, but for a February starting month there is a broad correlation peak from August to November (not shown) that might reflect an early reemergence (the deepest mixed layer is in February). As the autocorrelation strongly depends on the starting month indicates a lack of robustness, this box is blue in Fig. 7a, which indicates hints of reemergence. Further west, the (40°-35°W, 45°-50°N) box shows no indication of SSS reemergence (Fig. 5c) despite its large mixed layer depth range (Fig. A2), presumably because of very poor data coverage until mid-2001 (Fig. 3b). This box is ochre in Fig. 7a, which indicates no reemergence. SSS reemergence is seen, albeit noisy, (Fig. 5b) in the better sampled (50°-

45°W, 45°-50°N) box, with a correlation minimum in August followed by a broad increase peaking in March, even though the winter mixed layer is shallow and its seasonal range is only 15 m in Fig. A2. However, the range is larger in Carton et al. (2018). Reemergence also seems to occur in the (55°-50°W, 45°-50°N) box (Fig. 5a), where the mixed layer depth range is larger (70m, Fig. A2). These two boxes are purple in Fig. 7a. In summary, reemergence is seen in 5 out of the 8 boxes of the higher latitude band that we could consider.

In the 35°-40°N latitudinal band, the eastern box (25°-20°W) has a mixed layer seasonal range of ~100m (Fig. A2), good sampling (Fig. 2), an autocorrelation minimum in late summer and maximum between November and January (Fig. 5j). This clearly indicates SSS reemergence. Further west (40°-35°W), the mixed layer depth range is similar but sampling poorer, albeit rather evenly distributed in time, so that the correlation minimum in August and the peak in October and November also strongly suggest reemergence (Fig. 5i). On the other hand, there is no indication of SSS reemergence in (50°-45°W; Fig. 5h), where the winter mixed layer is very deep due to strong atmospheric cooling over the path of the North Atlantic current, leading to large subduction and obduction (Qiu and Huang 1995). Since SST reemergence is seen there (blue curve), the lack of a SSS reemergence peak probably results from poor sampling (Fig. 2). Finally there is no indication of SSS reemergence in the two westernmost boxes (Fig. 5f,g), although there are hints of it for different staring dates, as indicated in Fig. 7a.

Finally, the seasonal autocorrelations are shown for 5 boxes in the 20°-25° latitudinal band. SSS reemergence is seen in (45°-40°W) (Fig. 5n), where the maximum winter mixed layer is less than 100 m, the mixed layer depth range is 68 m, and an autocorrelation minimum in summer precedes a winter correlation peak. Less favorable conditions for reemergence are found to the east (Fig. 5m, 42 m range), where a reemergence peak is only clearly seen for a February starting date (not shown), and to the west (Fig. 5o, 55 m range). Nonetheless, since both cases have an autocorrelation minimum in summer, SSS reemergence is considered as clearly occurring (purple in Fig. 7a). There is also evidence of SSS reemergence in (70°-65°W) and (65°-60°W) (Fig. 5k, l), despite limited sampling, in particular in the latter box, and a small seasonal range of mixed layer variation (23 and 20 m, respectively). Indeed, an autocorrelation peak occurs around October and December, respectively, which corresponds well to the December mixed layer depth maximum (Fig. A1). Note that the autocorrelation minimum only occurs in September, several months after the mixed layer is shallowest (Fig. A1), but these boxes, at least in their southern part, are strongly influenced by a large freshwater influx in late summer primarily originating from the Amazon and the Orinoco and advected by the North Brazil Current (e.g., Foltz et al. 2015). They can also be strongly impacted by the occasional hurricanes in fall, so caution is required.

To document a whole latitudinal band, the seasonal SSS autocorrelation is shown for all the boxes between 40° and 45°N (Fig. 6, red curves). In this case, the starting month and detrending were selected to best show local SSS reemergence. East of 35°W, the seasonal range of mixed layer depth is larger than 100m (Fig. A2), and local SSS reemergence is clearly seen in the two easternmost boxes as the autocorrelation has a summer minimum and a winter peak for February and March starting dates (Fig. 6i,j), although is only appears for an April starting date in (35°-30°W) (Fig. 6h), perhaps because of poorer sampling (Fig. 2). Sampling is also limited further west until 60°W, in particular in (55°-50°W) where raw sampling is very poor. However, an early SSS correlation peak (from August to November) is seen in (50°-45°W, Fig. 6e) where the mixed layer depth range is large (94m). Because this correlation peak occurs much earlier than the maximum mixed layer depth, SSS reemergence is considered as only hinted at in Fig. 7a. Further west, a winter SSS reemergence peak is seen in (65°-60°W), despite a shallow winter mixed layer depth and limited seasonal range (38m). Note that a summer minimum is seen for an April starting date, but the winter peak is larger for a March one, which is thus displayed (Fig. 6b). Finally, the signature of SSS reemergence is seen in (70°-65°W), despite a limited seasonal range (Fig. 6a).

For further illustration, the seasonal SSS auto-correlations are also shown in Fig. A3 (red curves) in the whole 30°-35°N band. SSS reemergence likely occurs in (70°-65°W), (60°-55°W), and (40°-35°N), which have a rather large seasonal range of mixed layer depth (149 m, 106 m, and 77 m, respectively), but, except in (45°-40°W) for an April staring date (not shown), there is no sufficient evidence of it elsewhere. In particular, SSS reemergence clearly does not occur in the subtropical gyre east of 35°W, despite seasonal ranges of ~ 100 m.

We also estimated the SSS seasonal auto-correlations using the raw SSS data averaged in the 5°x5° boxes instead of the analyzed ones. As expected from much sparser and noisier data (Fig. 2 and 3), fewer boxes show evidence of SSS reemergence, and SSS reemergence only appears more clearly in the raw data in a few boxes (not shown).

For comparison, the corresponding seasonal SST anomaly autocorrelations are shown in Fig. 5 (blue curves) in the same 1993-2016 period. Note that the choice of detrending or not in Fig. 5 was based on SSS and may not be optimal for SST as trends can differ. Evidence of SST reemergence is seen, albeit often noisily, in panels (d), (e), (h), (m), (n), and (o). There are hints of SST reemergence in panel (a), (f), (i), (k), and (l) but no sufficient evidence of it in panels (b), (c), (g), and (j). Interestingly, the autocorrelation minimum in panels (k)and (l) occurs in July, earlier than for SSS, which is probably because the freshening influence from the tropics, has limited impact on SST. Our assessment of SST reemergence is summarized in Fig. 7c. SST reemergence is most clearly seen in the most of the northern and central parts of the domain. SST reemergence occur in the northeastern corner, where seasonal range of mixed-layer depth is large, as noted before. The reemergence of SST is not seen in the eastern part of the subtropical gyre between 30°N and 40°N, east of 40°W, nor in the subtropics west of 60°W. There is evidence of SST reemergence at many southern boxes, although the annual cycle of mixed-layer depth is rather small (Fig. A1).

Unfortunately, the 5° x 5° SSS data are too noisy to often detect SSS reemergence during the second year, which would require an auto-correlation minimum around month 18-20 (June to August) followed by a peak around month 23-26 (November to February). Nonetheless, there are hints of a second SSS reemergence in Fig. 5 (panels e and n) and Fig. 6 (panel g). Note that a second reemergence may also occur remotely because of advection by the mean currents, although we found little evidence of it (see below).

To reduce the influence of advection, measurement errors, data gaps, and small-scale features, we have considered SSS and SST anomalies averaged over broader, but reasonably homogeneous areas, namely the northeastern and southeastern parts of the domain, as well as the western and eastern halves of the subtropical gyre, and considered longer lags. Because of the larger areas, there is no gap in the anomaly time series. Figure 8 shows the lag correlations for a March starting date for the four domains after removing a linear trend to better distinguish interannual persistence from long-term fluctuations. Similar results are obtained for a February and April starting date (not shown). In the northeastern domain (40°-20°W, 40°-50°N), SSS anomalies are very persistent, yet a first, a second, and a third SSS anomaly reemergence peaks following relative summer minima are clearly visible, and there may even be a fourth one (Fig. 8a). The latter is also suggested for a February starting date, but not an April one, although longer lags should be considered to unambiguously detect a fourth peak. Hence, the large-scale wintertime SSS anomalies only decay very slowly in this region, recurring for several winters. By contrast, there is only a first, slightly earlier SST reemergence peak, noisy evidence of a second one, and none of a third peak. Note that a clear second SST anomaly reemergence peak was seen in a longer data set in a broadly similar region, albeit extending to 60°N (Deser et al. 2003, their Fig. 9).

In the western subtropical gyre region (60°-35°W, 30°-40°N), the SSS autocorrelation (Fig. 8b) has two peaks, one at month 10, 11, and 12 (October to December) and the other at month 20 and 21 (August and September). However, the second peak occurs closely after the minimum mixed-layer depth (in July) and much before the maximum entrainment rate (Carton et al. 2018); hence it does not reflect SSS reemergence, but low-frequency fluctuations or eddy noise. This is consistent with the 5°x5° results, since SSS reemergence was only found in the easternmost part of the subdomain (Fig. 7). On the other hand, a more robust first reemergence peak is found for the large-scale SST anomalies, again consistent with the 5° x 5° box results. There is also a second, albeit small, SST peak in October and November, which becomes significant when an even larger domain (70°-30°W, 20°-40°N) is considered (not shown).

In the eastern subtropical gyre region (35°-20°W, 30-40°N), there is no clear indication of a first reemergence for either SSS or SST anomalies (Fig. 8c), consistent with the 5° x5° results in Fig. 7. However, there is a SSS correlation peak at lag 23 (December) followed by a minimum between the following May to August, and a broad peak between lag 35 and 40 (December to May). Note also the SST correlation peak near lag 23 (November). Although unlikely in a 24-year record, it might perhaps reveal the presence of a second and, for SSS, a third reemergence since, as pointed out by a reviewer, if the mixed layer is especially deep when the anomaly is formed in the first winter, anomalously shallow in the second winter, and anomalously deep in the winter after that, the re-entrainment of anomalous temperature or salinity anomalies into the surface mixed layer would skip a year.

In southeastern region (50°-20°W, 20°-30°N), a first and a second SSS reemergence peak are seen in November and December relative to a slow decay, and even hint of a third one (larger for a February starting date, lost for an April one), albeit not significant, each of them following smaller summer values, albeit noisy during the first summer (Fig. 8d). On the other hand, only a first SST reemergence peak is clearly seen above the background of low-frequency variations. This indicates that the large-scale wintertime SSS anomalies decay faster than in the northeastern corner, consistent with the smaller winter mixed-layer depth and inertia.

*b. Link to subsurface salinity*

To link the SSS anomaly correlation peaks to the reemergence of subsurface salinity anomalies, the GLORYS2V4 reanalysis was used, but only the 2005-2018 period was considered because of the insufficient number of salinity profiles before many ARGO floats became available. To verify whether such period would be sufficiently long to detect reemergence, we first re-did the correlation analysis using our data set in the 2005-2016 period. Unfortunately, 12 years of 5°x5° data turned out to be insufficient to reproduce many results based on 24 years, showing instead noisy correlations for both SSS and SST anomalies. Hence, it was not surprising that using reanalyzed SSS or SST anomalies derived from GLORYS2V4 mostly showed little evidence of reemergence and often at different locations. This is consistent with the often-limited correlation between the two SSS anomaly data sets, which is due to differences in both sampling and analysis methods. Nonetheless, evidence of SSS reemergence was found in both data sets for several of the 5°x5° boxes in the northeastern and southeastern parts of the domain where the correlation between the data sets was typically $\sim 0.6$, and reemergence had been found in the longer 1993-2016 data.

To optimize the links with subsurface data, the reanalyzed SSS anomalies were considered in the 2005-2018 period in two somewhat larger regions, one in the southeast (35°-20°W, 20°-30°N) and the other in the northeast (30°-20°W, 45°-45°N), where the maximum mixed layer depth is ~ 100 and 120 m, respectively (Fig. A1). A depth-time diagram of the lag correlation with the averaged salinity anomalies in the upper 20 m was constructed for both a February and a March starting date at lag ranging between 0 and 24. Despite the short data duration (14 years), the results for (30°-20°W, 45°-45°N) clearly show that the SSS anomalies, which extend throughout the mixed layer in late winter, are capped by the seasonal thermocline in summer at lag 3 to 6 (i.e. June to September) and reappear at the surface in fall and winter when subsurface water is entrained in the deepening mixed layer, peaking at lag 8 to 10 (November to the following January) (Fig. 9, left). After the winter, the correlation keeps decreasing, presumably because of the large low-frequency SSS fluctuations found at this location. Interestingly, the subsurface salinity and SST (not shown) anomalies propagate downward, reflecting the large southwestward subduction in this area (Marshall et al. 1993; Qiu and Huang 1995). Similar results are obtained with a February starting date, or when using SSS instead of the 0-20 m salinity as basic time series. As expected from the limited number of salinity profiles in the pre-ARGO period, no reemergence is seen when the longer 1993-2016 reanalyzed data set is used. Similar results are obtained for the (30°-20°W, 45°-45°N) domain, but for deeper wintertime anomalies, with the reemergence of the subsurface SSS anomalies starting around October (lag 7), peaking in December (lag 9), and lingering throughout winter, again consistent with the mean seasonal cycle of the mixed layer depth (Fig. 9, right). In summary, this analysis demonstrates, based on the two locations, that SSS reemergence can be well detected using the lag seasonal correlation analysis.

*b. With advection*

To take advection into account, which could lead to non-local SSS reemergence by displacing the deep mixed-layer water after they are capped by the seasonal thermocline, we used the virtual float trajectories *F* described in section 2.3. As illustrated in Fig. 4, they reflect the mean near-surface circulation of the subtropical gyre, except in the northwestern corner east of the Grand Banks (box 47), where the mean flow results from the southward flowing Labrador Current. Further east, the northern boxes are located on the southern side of the confluence of the subtropical and subpolar gyres. As shown by the averaged 2-year trajectories in Fig. 4, float velocity strongly varies with location within the subtropical gyre, with a 12-month displacement from the first March typically ranging between five and up to ten 1° grid cells. There are substantial year-to-year fluctuations in the trajectories, as illustrated for 5 boxes by the mean 2-year trajectories of the virtual float emitted in each year. Note the larger dispersion of the mean trajectories at box 32 (65°-60°W, 35°-40°N), which reflects the large eddy activity in the vicinity of the Gulf Stream. Along each individual 2-year virtual float trajectory *F,* the monthly SSS anomaly (before or after quadratic detrending) is interpolated from the 1° x 1° objective SSS maps, yielding the data matrix *SSS(1:24, F, R)*, where *R* is the number of successive years providing initial conditions. Because of data gaps, *R* is not always equal to 22, and can be as low as 17. The SSS anomalies following geostrophic advection are obtained by averaging them along the floats issued from each 5° x 5° box, yielding the data matrix SSS'(1:24, R), which is used to calculate the seasonal cross-correlations. The same procedure is used for SST anomalies. It should be stressed that for simplicity the cross-correlations and possible remote reemergence are attributed to the 5° x 5° boxes where the virtual floats were issued. However, the reemergence along individual trajectories really occurs in broader regions spanned by the float trajectories, which overlap neighboring 5°x 5° boxes, with a dispersion even larger than shown in Fig. 4, where only the mean trajectories for each year are represented. In other words, remote reemergence takes place at a different location determined by the mean horizontal currents and their daily variability. However, as the spatial scale of SST or SSS anomalies is generally much larger than the water displacements before the first reemergence, both local and remote reemergence could well be found for the same box.

As illustrated in Fig. 6 for the 40°-45N° latitudinal band, remote SSS reemergence might occur along float trajectories issued from the (50°-45°W) box, which largely go eastward (Fig. 6e, blue curves). At short lag, displacement is limited and, as expected, the seasonal autocorrelation closely resembles that of the issuing box. However, the correlation maximum is slightly sharper and occurs one month earlier, although the maximum still occurs in October for a February starting month (not shown). Nonetheless, because the maximum mixed layer depth occurs in February, remote reemergence is considered as hinted at in Fig. 7b, as was the local one. Floats issued from (45°-40°W) do not appear to reemerge (Fig. 6f), despite a minimum correlation in June, and there is no reemergence evidence based on other starting months. The correlations based on floats issued from 40°-35°W are very sensitive to both starting month and detrending, but there is some tentative indication of possible reemergence for a February starting month (not shown). Remote reemergence seems to occur in 35°-30°W (Fig. 6h), but the correlation at large lag is affected by low-frequency variability, even with quadratic detrending. The same holds in 30°-25°W and 25°-20°W, although the reemergence signature is clearest for the latter box (Fig. 6i,j). In summary, good evidence of remote reemergence in 40°-45°N only occurs for floats issued east of 35°W. Interestingly, even at large lags the auto-correlations along float trajectories largely resemble the local ones in the issuing boxes, suggesting that the SSS anomalies have a large zonal scale.

In the 30°-35°N latitudinal band (Fig. A3, blue curves), taking advection into account enhances the detection of SSS reemergence for a few boxes, such as in panels (d) and (f). However, as summarized in Fig. 7b, taking advection into account somewhat deteriorates the detection of SSS reemergence in other areas. In particular, remote reemergence is only seen in a third of the boxes in the 45°-50°N band, in part because of limited data density (Fig. 2), and no SSS data availability north of 50°N when interpolating SSS along the trajectories that escape the domain (8 to 9%). Also, remote SSS reemergence is seldom identified for boxes west of 55°W, perhaps in part because of the large dispersion of the trajectories (see Fig. 4) caused by the strong eddy activity in the western North Atlantic. On the other hand, remote reemergence is more often found for trajectories issued from the central part of the domain, but less often for those issued at the southernmost locations.

Similarly, taking advection into account leads to fewer boxes with clear remote SST reemergence (Fig. 7d). Remote SST reemergence is found when issued from most of the northern boxes, but it is not as often clear between 40°N and 50°N. Also, remote SST reemergence is not clearly detected between 20°N and 25°N, west of 40°W, and is still not seen in much of the eastern subtropical gyre.

The reemergence along artificial float trajectories was also investigated in the larger domains, thus considering anomalies along all the float trajectories issued within them, although only lags up to month 24 (December) could be considered due to the limited duration of the trajectories (section 2). Consistent with the 5° x 5° results, advection generally degrades the detection of SSS reemergence, while only slightly affecting SST reemergence. This is particularly striking in the northeastern domain (Fig. 10a), where the first SSS reemergence peak is negligible and the second one is narrower, independent of the starting date (not shown). However, this may be due in part to the larger SSS anomaly persistence along the trajectories. In the western subtropics (Fig. 10b), the first remote SSS reemergence peak is stronger than the local one in Fig. 8b, while the second peak is smaller, still occurring too early (in October) for reemergence, and no remote SST reemergence is apparent. There is no convincing indication of SSS or SST reemergence along floats issued from the eastern subtropical region (Fig. 10c), but note that the SSS anomalies are very persistent. Finally, the first SST and SSS reemergence peaks for trajectories issued from the southeastern domain (Fig. 10d) are as large as without advection, but only hint of the second SSS reemergence peak remains. Hence, even for larger domains, taking advection into account mostly degrades reemergence detection.

## 4. Summary and discussion

The Atlantic SSS fields constructed from observations by RKFD07 have been extended to the 1970-2016 period. The raw SSS data are rather sparse, except along VOS lines and when many Argo floats became available. The monthly SSS was gridded in 30°S-50°N using objective mapping at 1°x1° spatial resolution. The reemergence of SSS anomalies was investigated between 20°N and 50°N during the 1993-2016 period, when the sampling was improved and surface geostrophic currents derived from satellite measurements became available. To do so, the objective fields were binned in 5°x5° squares if at least 3 values (among 25) were available. Although the binning results in rather complete data set for most boxes, it is based on raw data whose density often ranges between 10 and 35% before objective mapping. Hence, the monthly SSS anomaly fields have limited accuracy and are sensitive to eddy and instrumental noise. In addition, there are large low-frequency SSS fluctuations that may obscure reemergence in the short 24-year data set. Nonetheless, the new data set has allowed us to detect for the first time SSS reemergence in observations.

SSS reemergence was first investigated locally in each 5°x5° box, using seasonal auto-correlation functions with a February, March, or April starting month, in relation to the climatological seasonal cycle of the mixed layer depth. For comparison, the local SST anomaly reemergence was also investigated in the same 1993-2016 period. Although one expects that the SSS and SST autocorrelations should be broadly similar when there is reemergence, there were differences in the occurrence and the timing of the reemergence peak. This suggests that SSS and SST are affected differently by data availability, noise, and low-frequency fluctuations. In addition, SST and SSS anomalies should be affected differently by anomalous advection where the climatological SST and SSS gradients do not correspond, and by mean advection when their spatial scale differs.

The results were separated, albeit somewhat subjectively, into cases with clear reemergence, hints of possible reemergence, and no reemergence (Fig. 7). Both SSS and SST reemergence are clearly seen locally in most boxes of the northeastern corner, where the winter mixed-layer depth is deep (de Boyer et al. 2004; Carton et al. 2008; Sallée et al. 2021) and the seasonal range generally exceeds 100 m. Interestingly, the correlation between the wintertime SST and SSS anomalies is generally large (up to 0.66 in 30°-20°W, 45°-50°N), suggesting that they were largely driven by the same atmospheric fluctuations and/or similar low-frequency oceanic variability. Although the winter mixed-layer is rather shallow and the seasonal range limited, SSS and SST reemergence are largely seen in the southeastern part of the domain and, to a lesser extend, the northwestern corner. Puzzlingly, SSS reemergence was detected or hinted at in several boxes between 30°N and 40°N, west of 60°W, while no local SST reemergence was seen, although it was found in Deser et al. (2003), de Coëtlogon and Frankignoul (2003), and Hanawa and Sugimoto (2004) in longer data sets. On the other hand, there is limited evidence of SSS reemergence in the central part of the domain, presumably because of limited sampling since SST reemergence is largely found there. In the eastern subtropical gyre, east of 35°W, there is no SST reemergence nor, albeit in a narrower domain, SSS reemergence, as expected from a rather high correlation between SSS and SST anomalies. The lack of SST reemergence in the eastern subtropical gyre is consistent with previous studies (Deser et al. 2003; de Coëtlogon and Frankignoul 2003; Hanawa and Sugimoto 2004; Byju et al. 2018), and it has been attributed to oceanic subduction, strong oceanic heat loss, and, for the North Atlantic Madeira mode water (Sugimoto and Hanawa 2005), vigorous salt-finger mixing. A small seasonal range of mixed layer depth has also been invoked, but the range is actually large ~ 100 m and unlikely to be a contributing factor.

Overall, local SSS reemergence was detected in 27 of the 57 5°x5° boxes, and hinted at in 9 others, while SST reemergence was detected in 31 boxes and hinted at in 11 others. Hence, while SST reemergence is seen more often than SSS reemergence, the number of clear SST reemergence cases remains limited. This reflects in part the short duration (24 years) of the investigated period, which makes the correlation analysis sensitive to sampling errors and low frequency fluctuations and eddy noise.

To investigate longer spatial and temporal scales, and whether a second or third reemergence peak could be seen, the SSS and SST anomalies were averaged over broader domains, thus reducing the impact of data noise, small-scale fluctuations, and advection. In the northeastern region (40°-20°W, 40°-50°N), a first, a second and a third SSS reemergence peaks were seen, with even hints of a fourth one, resulting in a very long persistence (e-folding time of about 4 years) of the large-scale SSS anomalies in the cold season. As expected from the negative heat flux feedback (e.g., Frankignoul and Kestenare 2002) that damps SST anomalies when they are in contact with the atmosphere while SSS anomalies are little affected, the persistence of the wintertime SST anomalies is smaller, as noted by Alexander et al. (2011), and only a second SST reemergence peak, albeit noisy, could be seen. In the western subtropical gyre region (60°-35°W, 30°-40°N), only a first reemergence peak was seen for the SST anomalies and, less convincingly, the SSS anomalies, consistent with the 5°x5° box results. In the eastern subtropical gyre region (35°-20°W, 30-40°N), there was no first SSS or SST reemergence peak, as in the 5°x5° boxes, but there were peaks that could reflect a second and a third SSS reemergence, or be accidental in view of the lack of first reemergence. In the southeastern region (50°-20°W, 20°-30°N), a first, a second and hints of third reemergence peaks were found for the SSS anomalies, which thus decay faster than in the northeast, consistent with the smaller winter mixed-layer depth. In contrast, only a first SST reemergence could be clearly seen, reflecting again that wintertime SSS anomalies are more persistent than SST anomalies. In longer data sets, a second SST reemergence peak had been found for the main mode of North Atlantic SST variability, namely the North Atlantic SST anomaly tripole (Watanabe and Kimoto 2000; Deser et al. 2003; de Coëtlogon and Frankignoul 2003). However, as the EOF gives substantial weight to SST anomalies in both the northeastern and the southeastern domains, the second reemergence may reflect the behavior of the more persistent northeastern region.

To verify that the correlation peaks that we attributed to SSS reemergence correspond to the re-surfacing of the deep wintertime salinity anomalies by entrainment when the mixed layer is deepening, the GLORYS2v4 reanalysis was considered during the 2005-2018 period when ARGO floats lead to a large number of salinity profiles. Although in many 5°x5° boxes, the 2005-2016 period was often too short to show consistency between the seasonal correlations obtained from our data set and the reanalysis, or those obtained in the whole 1993-2016 period, there were several boxes in the northeastern and southeastern domains that showed consistent reemergence peaks. To optimize the relation with subsurface salinity data in these regions, averaged salinity anomalies were constructed for two larger domains, (35°-20°W, 20°-30°N) and (30°-20°W, 40°-45°N). At both sites, the correlation between late winter surface or near-surface salinity anomalies and subsurface salinity at increasing lag clearly showed that the late winter salinity anomalies are indeed capped by the seasonal thermocline during late spring and summer, and are then re-mixed in the surface mixed layer by entrainment during its fall deepening, leading to a winter correlation peak with the surface salinity in the previous winter. This confirms that SSS reemergence can indeed be well detected from SSS anomaly alone when the sampling is sufficiently large.

To take into account advection by the ocean currents that could lead to remote reemergence (rather than occurring locally), the analysis was also performed along a large ensemble of 24-month virtual float trajectories based on the daily estimates of the AVISO surface geostrophic currents. However, this neglects geostrophic shear, perhaps leading to an overestimate of the advection during summer, as well as Ekman currents, which may play a role in late autumn and winter when the mixed layer is deep. It also neglects vertical advection, which may be large in regions of strong subduction or obduction This may explain why, contrary to expectations, there were fewer 5°x5° boxes for which remote SSS and SST reemergence could be clearly identified. In particular, there was much less evidence of SSS reemergence along trajectories issued in the 45°-50°N band, likely because of limited data density and no SSS data availability north of 50°N when interpolating SSS along the trajectories that escape the domain (8 to 9%), and perhaps also because of our use of surface geostrophic currents, although remote SST reemergence was largely seen. Little remote SSS or SST reemergence was clearly identified for anomalies issued west of 55°W, perhaps because of the larger dispersion of the trajectories caused by the strong eddy activity in the western North Atlantic. On the other hand, remote SSS reemergence was better seen along trajectories issued in the central part of the basin than local one. Along trajectories issued from boxes between 20°N and 25°N, little remote SSS reemergence was detected, and clear remote SST reemergence only seen west of 40°W, as in de Coëtlogon and Frankignoul (2003). This may be linked to shallower mixed layers and small seasonal mixed-layer depth range (Byju et al. 2018, Fig. A2) south of 20°N. Overall, remote SSS reemergence was clearly seen when issued from 21 boxes instead of being seen locally in 24 boxes (in the same domain). Similarly, there were fewer clear cases of remote SST reemergence (21 versus 29), although more cases with hints of remote SST reemergence.

Remote reemergence along the artificial float trajectories was also investigated for the four large domains, although shorter lags could only be considered because of the limited duration of the trajectories. Consistent with the analysis based of 5° x 5° boxes, taking advection into account generally tended to degrade the detection of large-scale SSS reemergence. However, it did not substantially affect the detection of SST reemergence, presumably because of the better SST data.

This study has focused on the detection of SSS anomaly reemergence and persistence in a purely observational data set, while the implications of our results for ocean circulation remain to be explored. Unfortunately, poor data coverage prevented us from considering SSS anomalies in the subpolar regions, where they critically affect the subpolar gyre and the meridional overturning circulations. Better coverage will be provided in the future by satellite-derived SSS products such as the weekly or monthly CCI SSS (multi-mission SSS product from the climate change initiative (Sea_Surface_Salinity_cci v2.31) project (doi:10.5285/4ce685bff631459fb2a30faa699f3fc5), but the time series are too short at present. However, such analysis could be attempted using reanalyzed products, oceanic model hindcasts, and climate models, with the present results used as a benchmark for validating them.

*Acknowledgements*

Support on SSS data acquisition and validation by SNO SSS, support by TOSCA /CNES SMOS and (to CF) the Office of Science of the US Department of Energy (DE-SC0019492) are gratefully acknowledged. We are grateful to Jean-Baptiste Sallée for providing the mixed layer data, and to Brady Fester and Simona Flavoni for making the mixed layer depth calculations. We thank Young-Oh Kwon, Jian Lu, Glenn Liu, and Jim Carton for useful comments, and the three anonymous reviewers for their constructive comments that substantially improved earlier versions of the manuscript. The gridded Sea surface salinity data is made freely available by the French Sea Surface Salinity Observation Service (http://sss.sedoo.fr/#GriddedProductMetadataPlace:ATLANTIC).

## Appendix 1: Climatological mixed layer depth

Sallée et al. (2021) have estimated the global seasonal cycle of the mixed layer depth on a 0.5°x0.5° grid, using temperature and salinity profiles from a number of different sources between 1970 and 2018, and a density threshold of 0.03 kg $m^{-3}$. After removing the mean seasonal cycle, the SSS anomalies were binned into the 5°x5° North Atlantic boxes used in this study, providing key information for reemergence. Figure A1 shows the maximum and the minimum mixed layer depth with their month of occurrence, and Figure A2 gives the range of seasonal mixed layer variations. However, as they reflect spatially averaged properties, values within each box may have much larger ranges.

## Appendix 1: Seasonal auto-correlation in 30°-35°N

## References

Alexander, M. A., and C. Deser, 1995: A mechanism for the recurrence of wintertime midlatitude SST anomalies. *J. Phys. Oceanogr.*, 25, 122–137.

Alexander, M. A., C. Deser, and M. S. Timlin, 1999: The reemergence of SST anomalies in the North Pacific Ocean. *J. Climate*, 12, 2419–2433.

——, M. S. Timlin, and J. D. Scott, 2001: Winter-to-winter recurrence of sea surface temperature, salinity and mixed layer depth anomalies. *Prog. Oceanogr.,* 49, 41–61.

Buckley, M.W. and J. Marshall, 2016 : Observations, inferences, and mechanisms of the Atlantic Meridional Overturning circulation : a review. *Rev. Geophys*., 54, 5-63.

Byju, P., D. Dommenget, and M.A. Alexander, 2018 : Widespread reemergence of sea surface temperature anomalies in the global oceans, including tropical regions forced by reemerging winds. *Geophys. Res. Lett.,* 45, 7683–7691. https://doi.org/10.1029/2018GL079137.

Carton, J.A., S.A. Grodsky, and H. Liu, 2008: Variability of the oceanic mixed layer, 1960-2004. *J. Climate*, 21, 1029-1047.

de Coëtlogon, G. and C. Frankignoul, 2003: The persistence of winter sea surface temperature in the North Atlantic. *J. Climate*, 16, 1364-1377.

de Boyer Montégut, C., G. Madec, A.S. Fisher, A. Lazar, and D. Iudicone, 2004: Mixed layer depth over the global ocean: An examination of profile data and a profile-based climatology. *J. Geophys. Res*. 109, CI2003, doi:10.1029/2004JC002378.

Deser, C., M. Alexander, and M. Timlin, 2003: Understanding the persistence of sea surface temperature anomalies in midlatitudes. *J. Climate*, 16, 57–72.

Dibarboure G., and co-authors, 2011: Jason-2 in DUACS: first tandem results and impact on processing and products. *Marine Geodesy Jason-2 Special Issue, Vol 2. 34*, 214-241.

Frankignoul, C. and E. Kestenare, 2002: The surface heat flux feedback. Part 1: Estimates from observations in the Atlantic and the North Pacific. *Clim. Dyn*., 19, 633-647.

Good, S.A., M.J. Martin, and N. A. Rayner, 2013: EN4: Quality controlled ocean temperature and salinity profiles and monthly objective analyses with uncertainty estimates. *J. Geophys. Res.: Oceans*, 118, 6704-6716 doi. 10.1002/2013JC009067.

Grist, J.P., and co-authors, 2019: Re-emergence of North Atlantic subsurface ocean temperature anomalie in a seasonal forecast system. *Clim. Dyn*. 53, 4799-4820.

Hanawa, K., and S. Sugimoto, 2004: Reemergence areas of winter sea surface temperature anomalies in the world's oceans. *Geophys. Res. Lett.*, 31, L10303, doi:10.1029/2004GL019904.

Ishii, M., M. Kimoto, K. Sakamoto, and S.-I. Iwasaki, 2006: Steric sea level changes estimated from historical ocean subsurface temperature and salinity analyses. *J. Oceanography,* 62, 155-2006.

Marshall, J.C., A.G. Nurser, and R.G. Williams, 1993; Inferring the sudduction rateand period over the North Atlantic. *J. Phys. Oceanogr.*, 23, 1315-1329.

Murata, K., S. Kido, and T. Tozuka, 2020 : Role of reemergence in the central North Pacific revealed by a mixed layer heat budget analysis. *Geophys. Res Lett.*, 47, e2020GL088194. https://doi.org/10.1029/2020GL088194

Namias, J., and B. M. Born, 1970: Temporal coherence in North Pacific sea-surface temperature patterns. *J. Geophys. Res.*, 75, 5952–5955.

Reynolds R.W., N.A. Rayner, T.M. Smith, D.C. Stokes D.C., and W. Wang, 2002: An improved in situ and saltellite SST analysis for climate, *J. Climate, 15,* 1609-1625.

Qiu, B. and R.X. Huang, 1995: Ventilation of the North Atlantic: Subduction versus obduction. *J. Phys. Oceanogr.*, 25, 2374-2390.

Reverdin, G., E. Kestenare, C. Frankignoul, and T. Delcroix, 2007: Surface salinity in the Atlantic Ocean (30°S-50°N). *Progr. Oceanogr.*, 73, 3011-3140.

Sallée, J.-B., and co-authors, 2021: Summertime increase in upper ocean stratification and mixed layer depth. *Nature*, 591, 592-598.

Sugimoto, S. and K. Hanawa, 2005: Why does reemergence of winter sea surface temperature anomalies not occur in eastern mode water areas? *Geophys. Res. Lett.* 32, L15608, doi:10.1029/2004GL021410.

Sugimoto, S. and K. Hanawa, 2007: Impact of remote reemergence of the subtropical mode water on winter SST variation in the central North Pacific. *J. Climate*, 20, 173-186.

Taws, S.L., R. Marsh, N.C. Wells, and J. Hirschi, 2011: Re-emerging ocean temperature anomalies in late-2010 associated with a repeat negative NAO. *Geophys. Res. Lett.*, 38, L20601, doi:10.1029/2011GL048978.

Timlin, M., M. Alexander, and C. Deser, 2002: On the reemergence of North Atlantic SST anomalies. *J. Climate*, 15, 2707–2712.

Watanabe, M. and M. Kimoto, 2000: On the persistence of decadal SST anomalies in the North Atlantic. *J. Climate*, 13, 3017-3028.

Zhang, R., 2017: On the persistence and coherence of subpolar sea surface temperature and salinity anomalies associated with the Atlantic multidecadal variability. Geophys. Res. Lett., 44, doi :10.1002/2017GL074342.

Zuo, H., M. Balmaseda, S. Tietsche, K. Mogensen, and M. Mayer: The ECMWF operational ensemble reanalysis-analysis system for ocean and sea-ice:Adescription of the system and assessment. *Ocean Sci. Discuss.,* https://doi.org/10.5194/os-2018-154.

## Figure captions

Figure 1. (Top) Time evolution of the number of 1° x 1° grid points per year included in the analysis as a function of year for 1970-2016 (there are on the order of 65,000 grid points-months in a year) and (Bottom) their spatial distribution, in number of months with SSS observations (564 if each month had data) (http:// dx.doi.org/10.6096/SSS-LEGOS-GRID-ATL).

Figure 2. Percentage of data points in each 5° x 5° box before (left) and after (right) objective analysis for the 1993-2016 period.

Figure 3. Time series of the average monthly SSS anomalies in various 5°x5° boxes before (yellow) and after (blue) objective analysis. Their location and number of monthly estimates (among 288) are indicated. Red indicates that the objective analysis provided less than 3 values.

Figure 4. Mean 2-year trajectory (black lines) of the virtual floats issued in March from each 5° x 5° box. The mean trajectory of the virtual floats deployed in each of the 22 successive 2-years are shown in different colors for five selected boxes.

Figure 5. Seasonal auto-correlation starting in March for various boxes without or with quadratic detrending, as indicated. The box location is given. The x-axis indicates the months of the year, not the lag (for instance, months 3 and 15 indicate March). Red is for SSS and blue for SST. The 10% significance level for complete data is indicated (dashed line).

Figure 6. Seasonal auto-correlation following the time-varying surface geostrophic flow (in blue) and estimated locally (in red) for the (40°-45N°) boxes (location is indicated). The starting month is March and a linear trend is removed, unless another month or quadratic detrending (as indicated) gave better evidence of local SSS reemergence. The x-axis indicates the months of the year, not the lag (for instance, months 3 and 15 indicate March). The 10% significance level for complete data is indicated (dashed line).

Figure 7. Estimation of (top) SSS and (bottom) SST reemergence at each 5° x 5° box (left) locally and (right) along mean surface flow trajectories. The color indicates whether reemergence is clearly seen (purple), possible (blue), or not found (ochre). Boxes with

insufficient data are shown in white. The starting months for which reemergence is detected are indicated (F for February, M for March and A for April).

Figure 8. Seasonal auto-correlation starting in March for detrended averaged SSS and SST anomalies in larger regions, as indicated. The x-axis indicates the months of the year (for instance, months 3, 15, 27 and 39 indicate March). Red is for SSS and blue for SST. The 10% significance level is indicated (dashed line).

Figure 9. Seasonal correlation (shaded, scale at left) starting in March in the (left) (35°-20°, 20°-30°N) and (right) (30°-20°W, 40°-45°N) regions between the salinity averaged over 0-20m and salinity at the upper 35 levels of the GLORYS2V4 reanalysis. The x-axis indicates the months of the year (for instance, months 3 and 15 indicate March) in the 2005-2018 period. The 10% significance level is 0.47 until lag 9 and 0.48 until lag 21.

Figure 10. Seasonal auto-correlation of detrended SSS and SST anomalies advected along the surface geostrophic flow for larger regions, as indicated. The x-axis indicates the months of the year (for instance, months 3, 15, 27 and 39 indicate March). Starting date is March; red is for SSS and blue for SST. The 10% significance level is indicated (dashed line).

Figure A1. Mean monthly maximum (left) and minimum (right) climatological mixed layer depth together with the month of occurrence, based on the data by Sallée et al. 2021.

Figure A2. Range (in m) of the seasonal cycle of the climatological mixed layer depth based on the data by Sallée et al. 2021.

Figure A3. Seasonal auto-correlation following the time-varying surface geostrophic flow (in blue) and estimated locally (in red), starting in March for the (30°-35°N) boxes. Their location is indicated. The x-axis indicates the months of the year, not the lag. No trend has been removed. The 10% significance level for complete data is indicated (dashed line)

## Figures

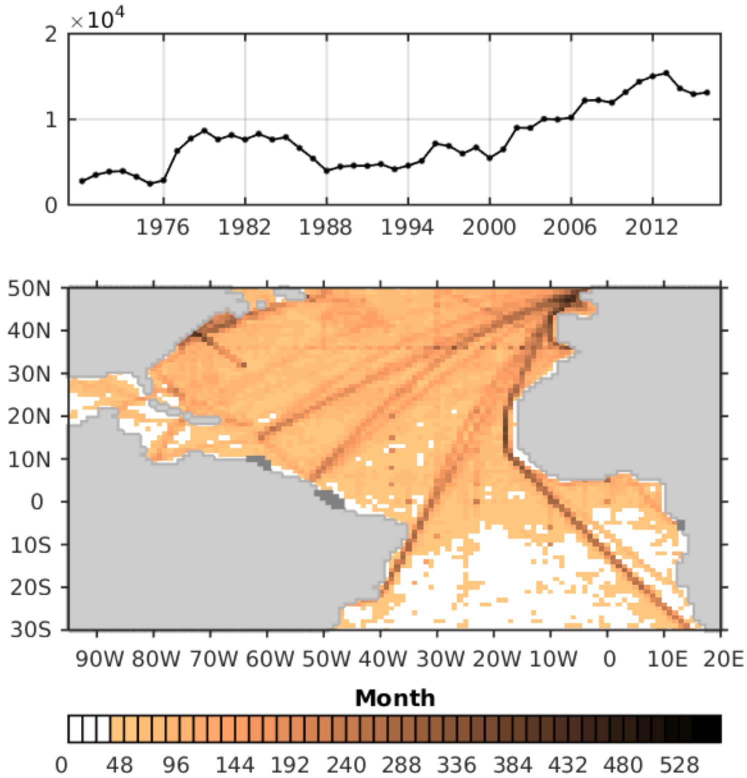


Figure 1. (Top) Time evolution of the number of 1° x 1° grid points per year included in the analysis as a function of year for 1970-2016 (there are on the order of 65,000 grid points-months in a year) and (Bottom) their spatial distribution, in number of months with SSS observations (564 if each month had data) (http:// dx.doi.org/10.6096/SSS-LEGOS-GRID-ATL).

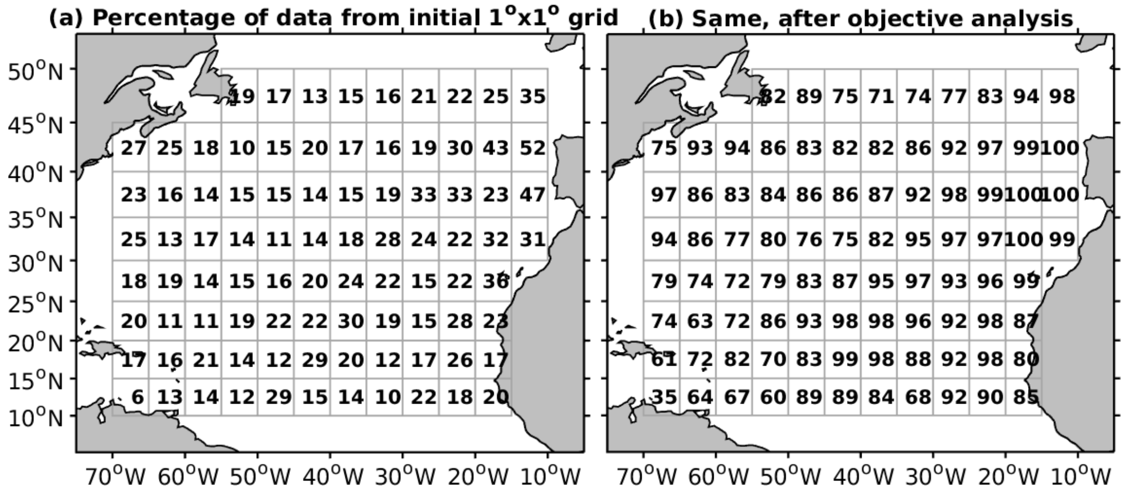


Figure 2. Percentage of data points in each 5° x 5° box before (left) and after (right) objective analysis for the 1993-2016 period.

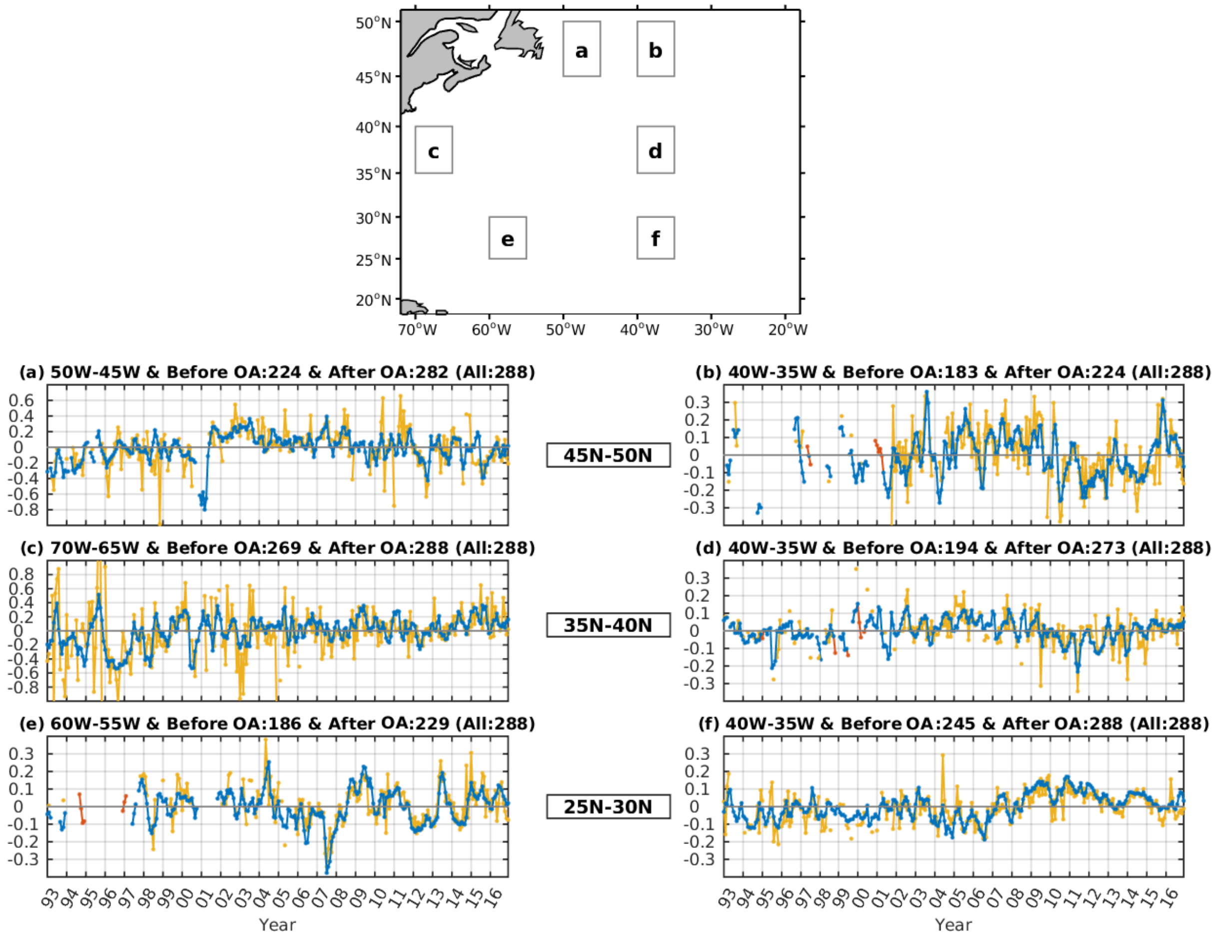


Figure 3. Time series of the average monthly SSS anomalies in various 5°x5° boxes before (yellow) and after (blue) objective analysis. Their location and number of monthly estimates (among 288) are indicated. Red indicates that the objective analysis provided less than 3 values.

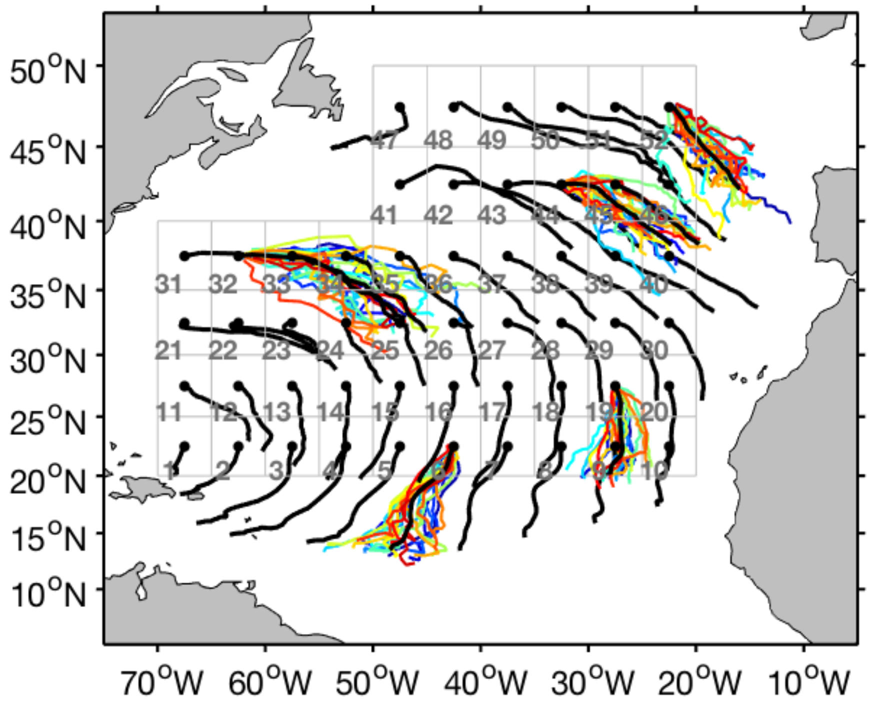


Figure 4. Mean 2-year trajectory (black lines) of the virtual floats issued in March from each 5° x 5° box. The mean trajectory of the virtual floats deployed in each of the 22 successive 2-years are shown in different colors for five selected boxes.

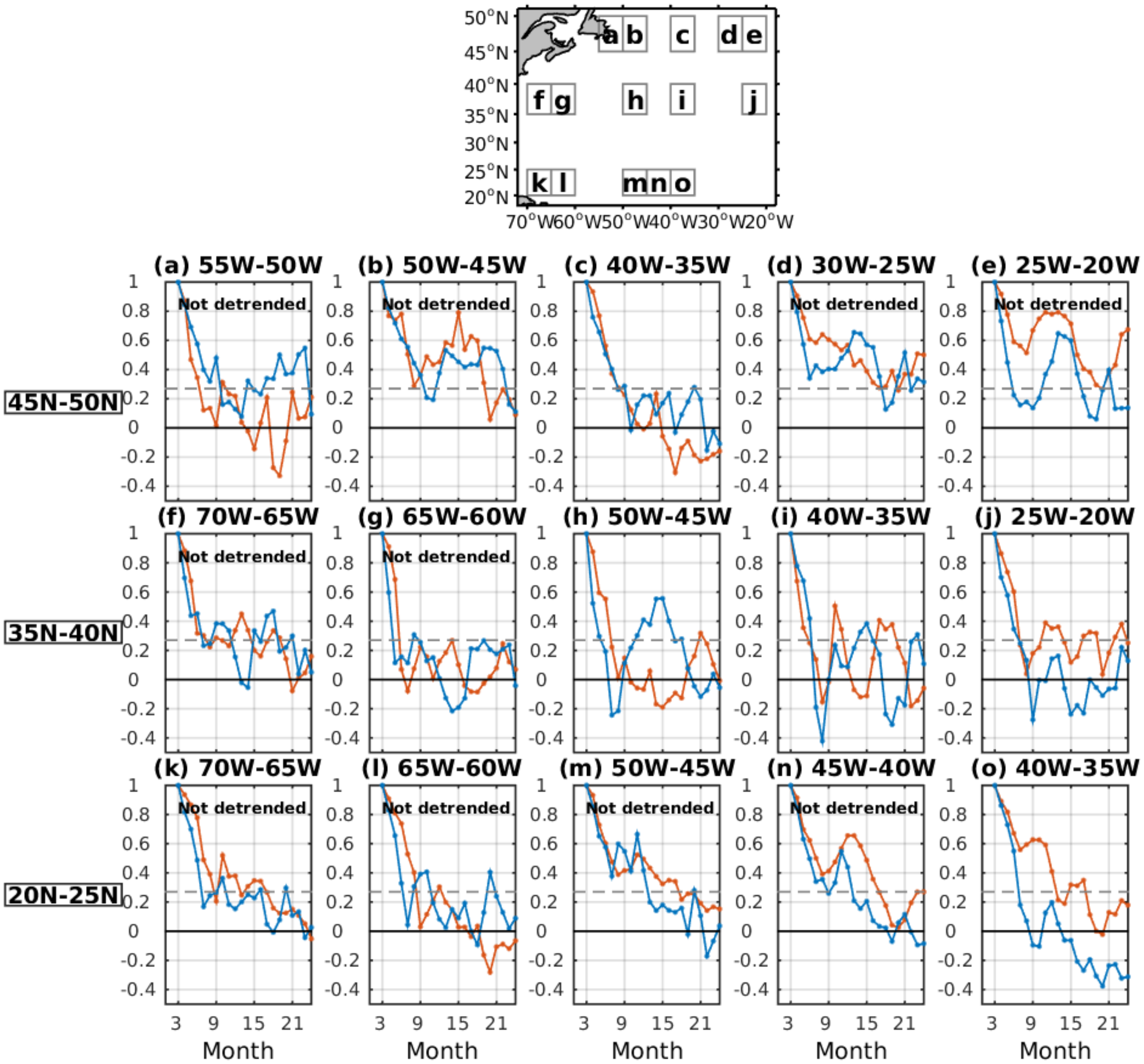


Figure 5. Seasonal auto-correlation starting in March for various boxes without or with quadratic detrending, as indicated. The box location is given. The x-axis indicates the months of the year, not the lag (for instance, months 3 and 15 indicate March). Red is for SSS and blue for SST. The 10% significance level for complete data is indicated (dashed line)

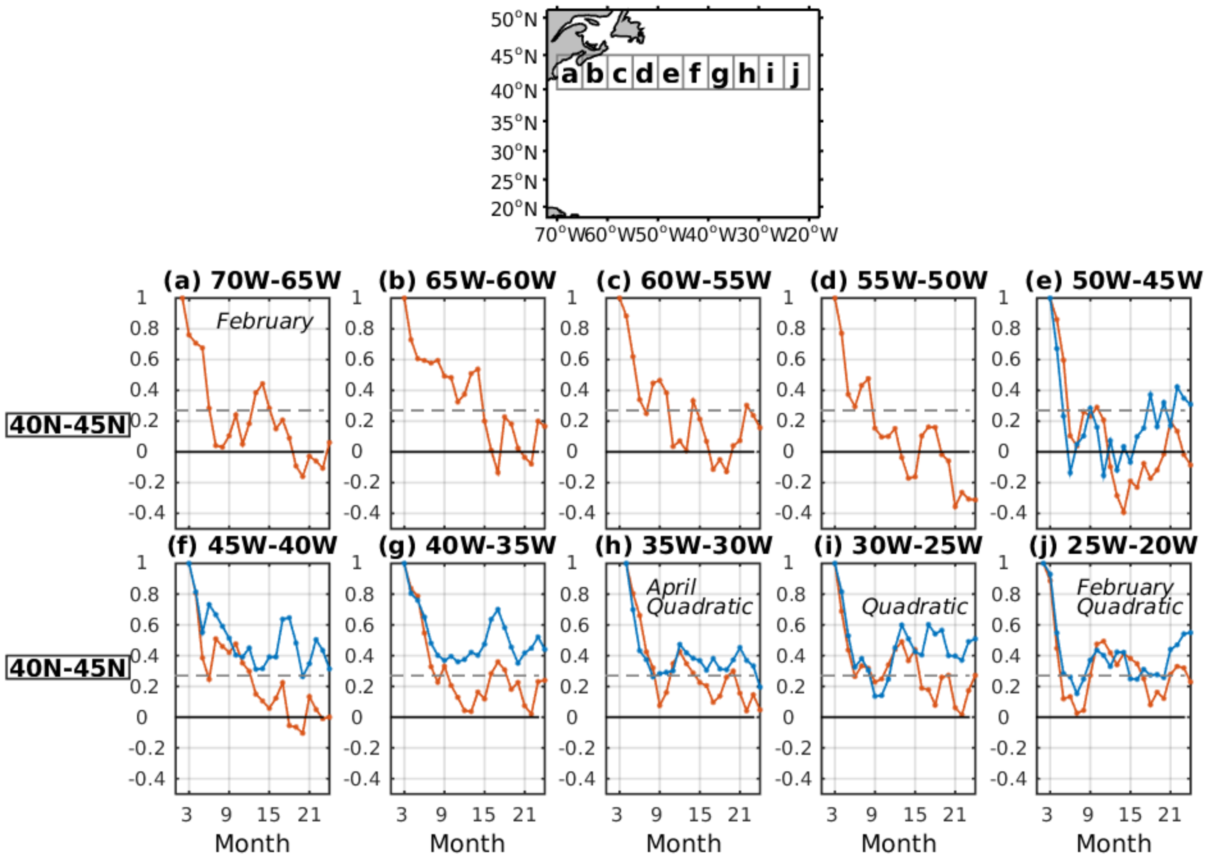


Figure 6. Seasonal auto-correlation following the time-varying surface geostrophic flow (in blue) and estimated locally (in red) for the (40°-45N°) boxes (location is indicated). The starting month is March and a linear trend is removed, unless another month or quadratic detrending (as indicated) gave better evidence of local SSS reemergence. The x-axis indicates the months of the year, not the lag (for instance, months 3 and 15 indicate March). The 10% significance level for complete data is indicated (dashed line).

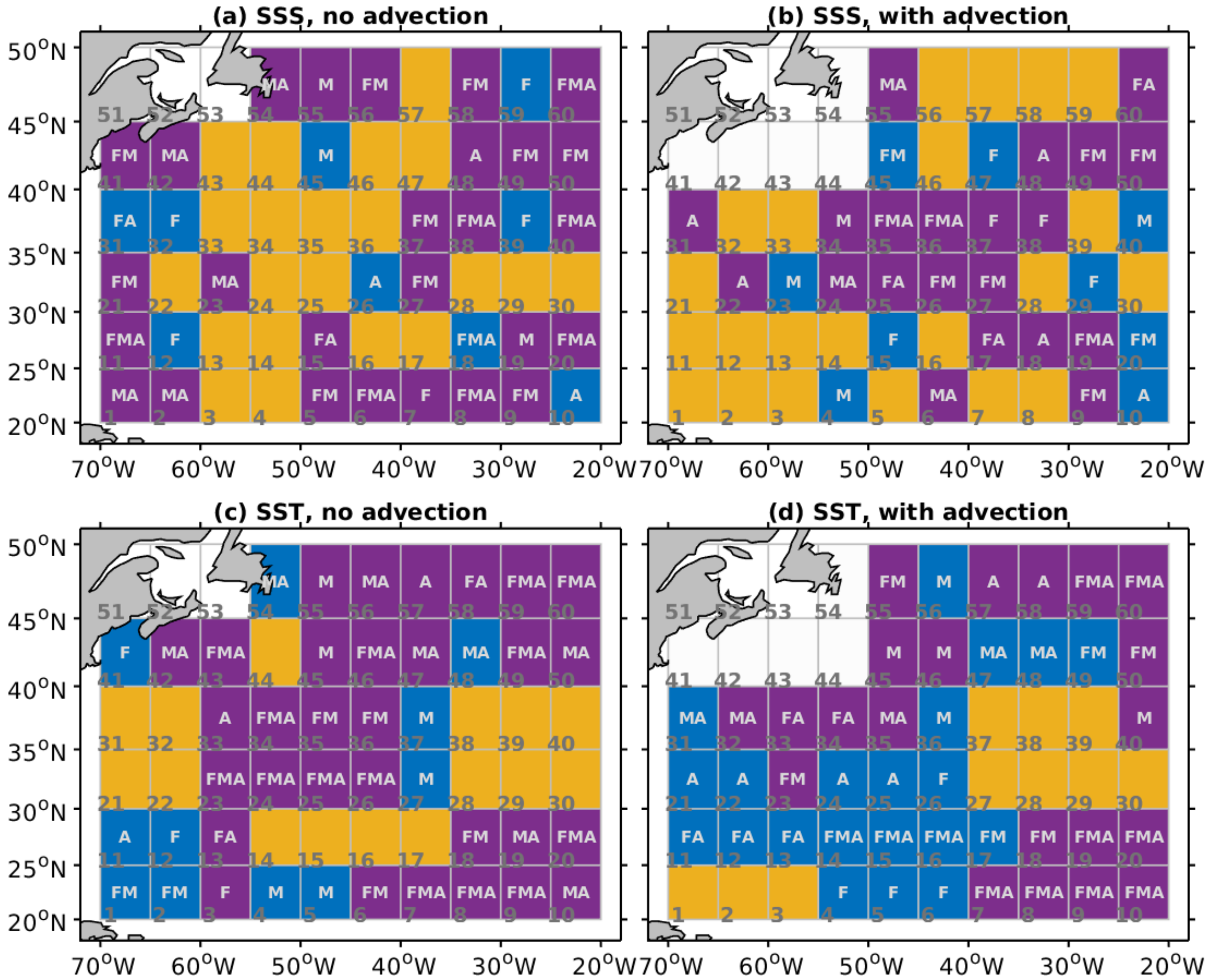


Figure 7. Estimation of (top) SSS and (bottom) SST reemergence at each 5° x 5° box (left) locally and (right) along mean surface flow trajectories. The color indicates whether reemergence is clearly seen (purple), possible (blue), or not found (ochre). Boxes with insufficient data are shown in white. The starting months for which reemergence is detected are indicated (F for February, M for March and A for April).

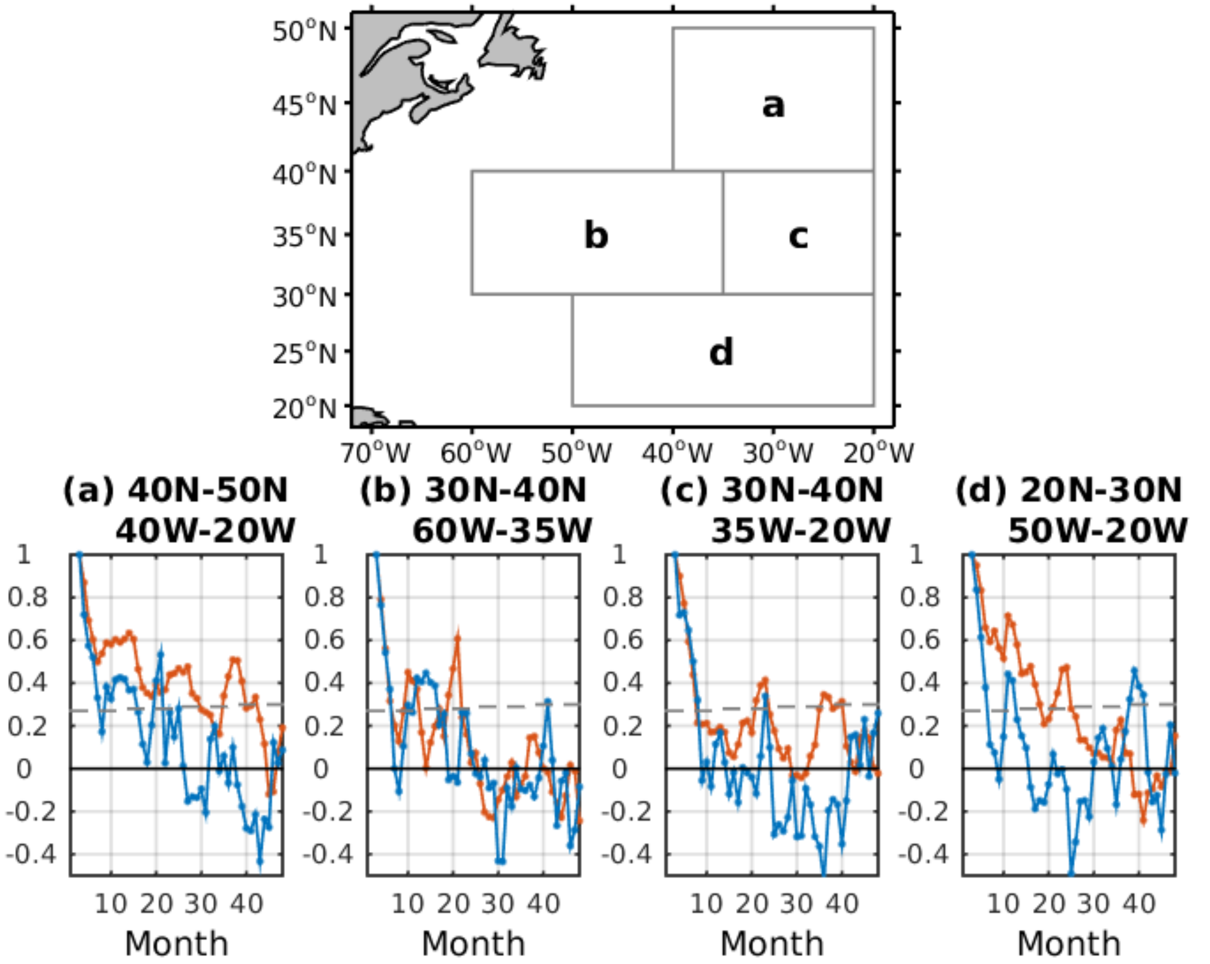


Figure 8. Seasonal auto-correlation starting in March for detrended averaged SSS and SST anomalies in larger regions, as indicated. The x-axis indicates the months of the year (for instance, months 3, 15, 27 and 39 indicate March). Red is for SSS and blue for SST. The 10% significance level is indicated (dashed line).

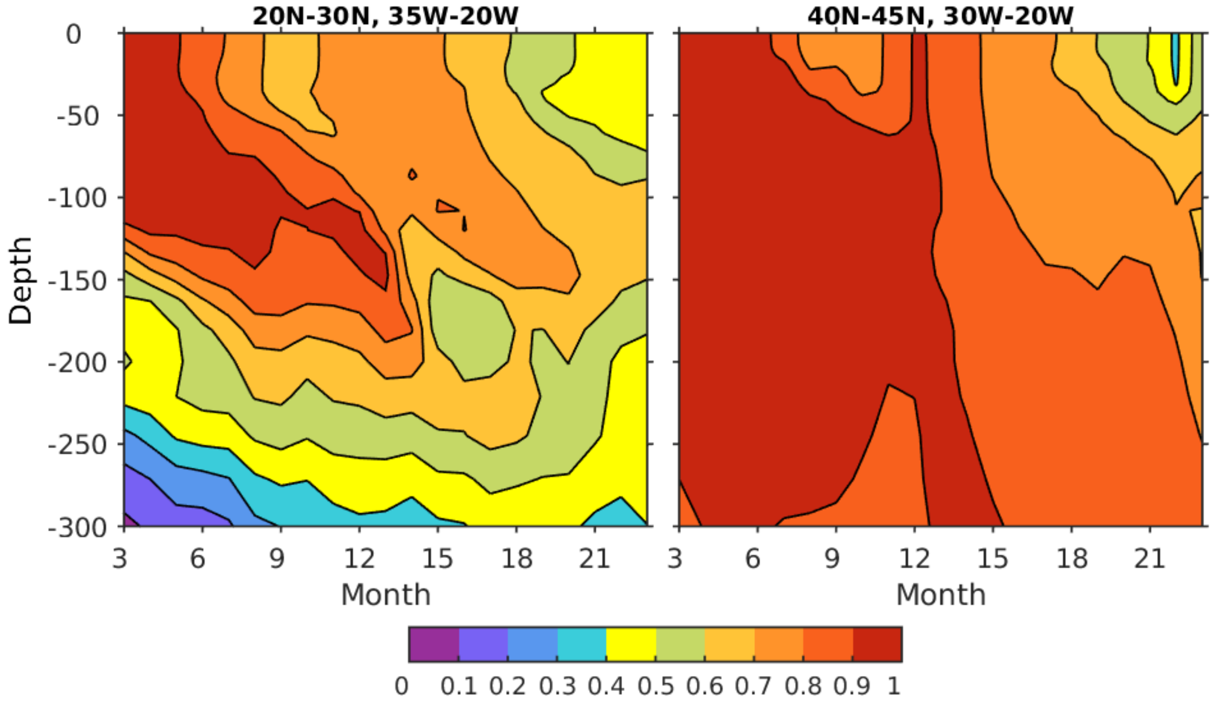


Figure 9. Seasonal correlation (shaded, scale at left) starting in March in the (left) (35°-20°, 20°-30°N) and (right) (30°-20°W, 40°-45°N) regions between the salinity averaged over 0-20m and salinity at the upper 35 levels of the GLORYS2V4 reanalysis. The x-axis indicates the months of the year (for instance, months 3 and 15 indicate March) in the 2005-2018 period. The 10% significance level is 0.47 until lag 9 and 0.48 until lag 21.

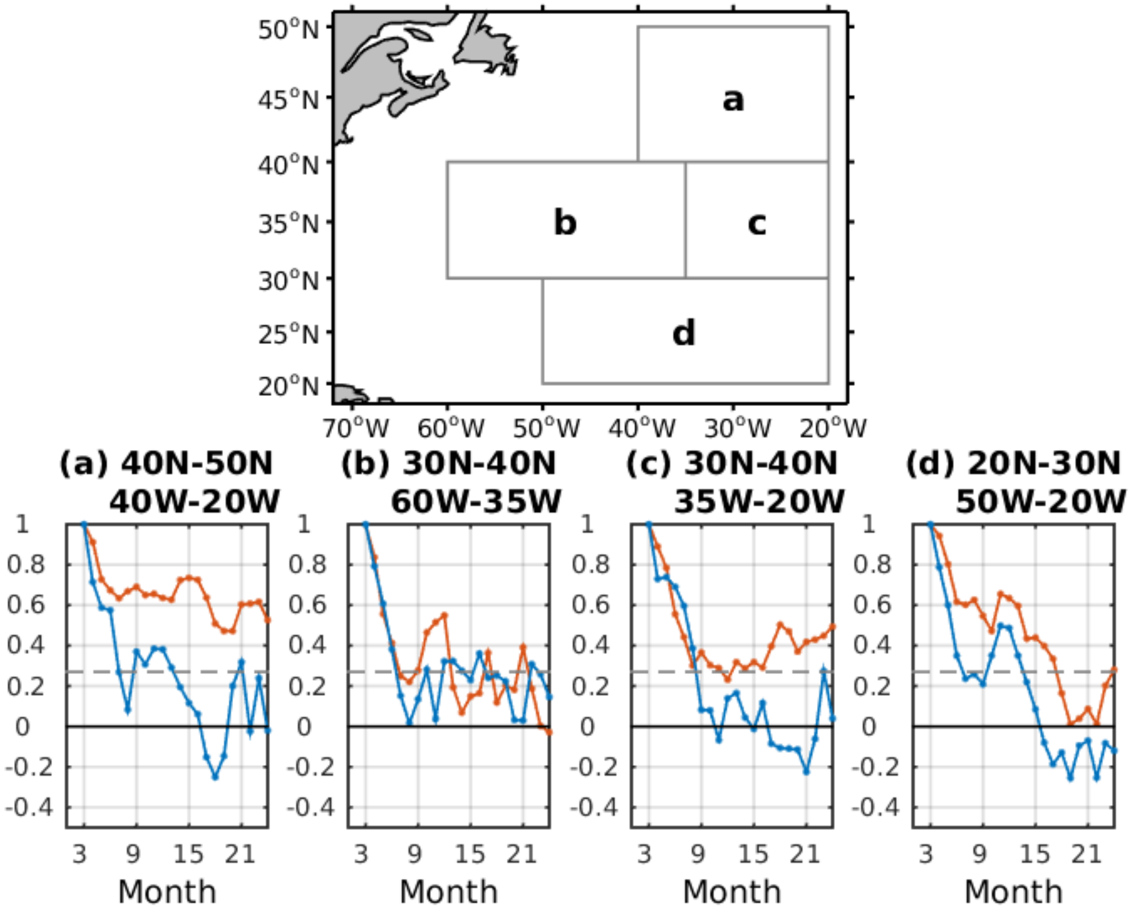


Figure 10. Seasonal auto-correlation of detrended SSS and SST anomalies advected along the surface geostrophic flow for larger regions, as indicated. The x-axis indicates the months of the year (for instance, months 3, 15, 27 and 39 indicate March). Starting date is March; red is for SSS and blue for SST. The 10% significance level is indicated (dashed line).

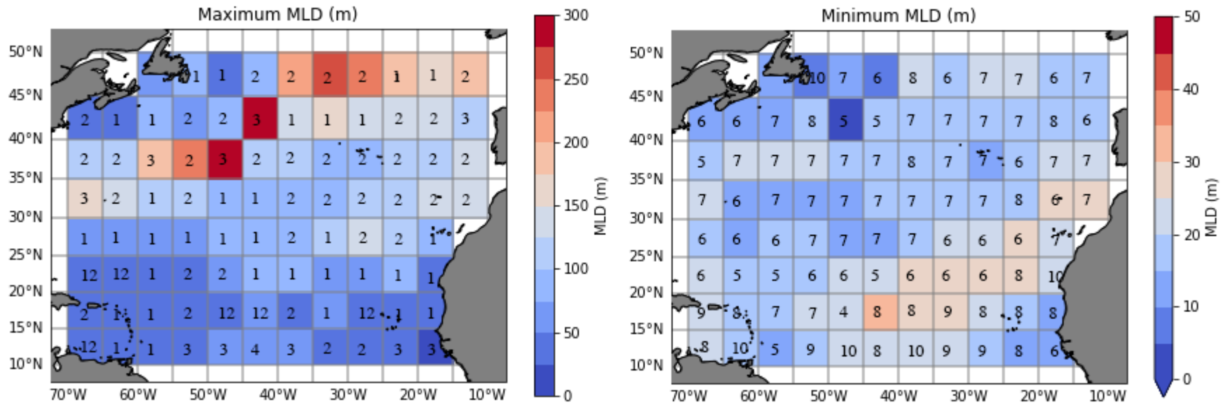


Figure A1. Mean monthly maximum (left) and minimum (right) climatological mixed layer depth together with the month of occurrence based on the data by Sallée et al. 2021.

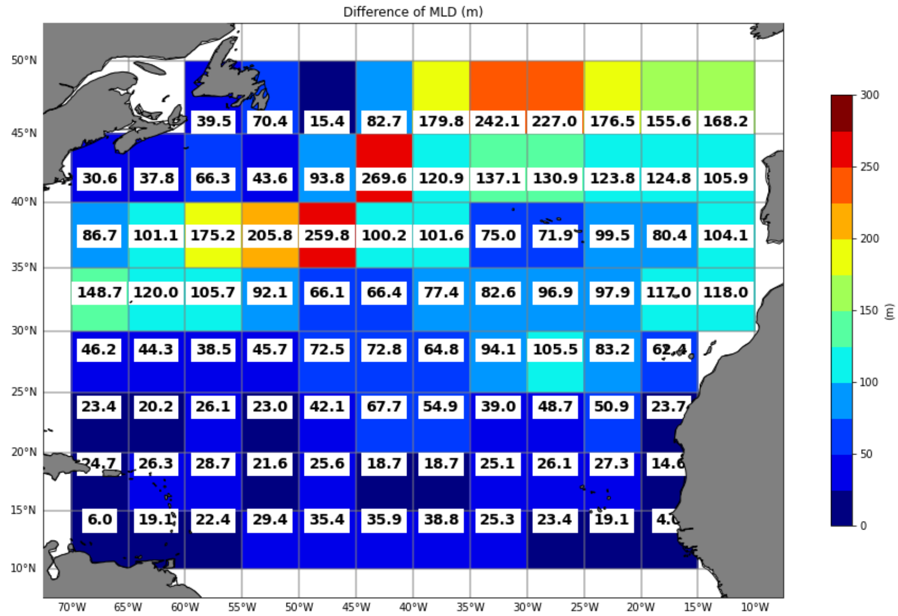


Figure A2. Range (in m) of the seasonal cycle of the climatological mixed layer depth based on the data by Sallée et al. 2021.

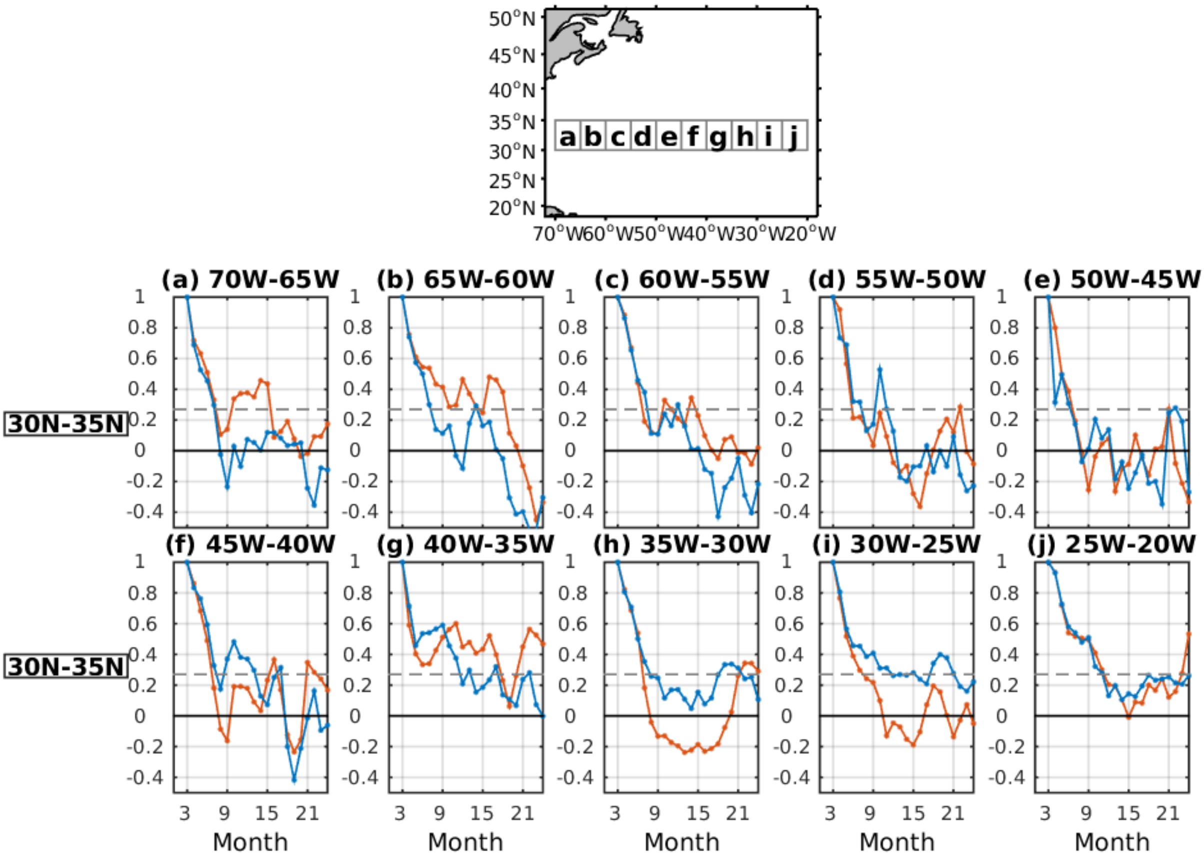


Figure A3. Seasonal auto-correlation of SSS following the time-varying surface geostrophic flow (in blue) and estimated locally (in red), starting in March for the (30°-35°N) boxes. Their location is indicated. The x-axis indicates the months of the year, not the lag. No trend has been removed. The 10% significance level for complete data is indicated (dashed line)